# Correlation between structural and opto-electronic characteristics of crystalline Si microhole arrays for photonic light management

Tobias Sontheimer, Veit Preidel, Daniel Lockau, Franziska Back, Eveline Rudigier-Voigt, Bernd Löchel, Alexei Erko, Frank Schmidt, Alexander Schnegg, Klaus Lips, Christiane Becker, and Bernd Rech

Citation: Journal of Applied Physics **114**, 173513 (2013); doi: 10.1063/1.4829008
View online: http://dx.doi.org/10.1063/1.4829008
View Table of Contents: http://scitation.aip.org/content/aip/journal/jap/114/17?ver=pdfcov
Published by the AIP Publishing

# Correlation between structural and opto-electronic characteristics of crystalline Si microhole arrays for photonic light management

Tobias Sontheimer,[1,a)] Veit Preidel,[1,2] Daniel Lockau,[1,3] Franziska Back,[4] Eveline Rudigier-Voigt,[4] Bernd Löchel,[5] Alexei Erko,[5] Frank Schmidt,[3] Alexander Schnegg,[1] Klaus Lips,[1] Christiane Becker,[1,2] and Bernd Rech[1]

[1]*Helmholtz-Zentrum Berlin für Materialien und Energie, Institute Silicon Photovoltaics, Kekuléstr. 5, Berlin 12489, Germany*
[2]*Helmholtz-Zentrum Berlin für Materialien und Energie, Si-Nanoarchitectures for Photovoltaics and Photonics, Kekuléstr. 5, Berlin 12489, Germany*
[3]*Konrad-Zuse-Zentrum für Informationstechnik Berlin, Takustraße 7, Berlin 14195, Germany*
[4]*SCHOTT AG, Hattenbergstraße 10, Mainz 55122, Germany*
[5]*Helmholtz-Zentrum Berlin für Materialien und Energie, Institute for Nanometre Optics and Technology, Albert-Einstein-Str. 15, Berlin 12489, Germany*

(Received 10 September 2013; accepted 21 October 2013; published online 7 November 2013)

By employing electron paramagnetic resonance spectroscopy, transmission electron microscopy, and optical measurements, we systematically correlate the structural and optical properties with the deep-level defect characteristics of various tailored periodic Si microhole arrays, which are manufactured in an easily scalable and versatile process on nanoimprinted sol-gel coated glass. While tapered microhole arrays in a structured base layer are characterized by partly nanocrystalline features, poor electronic quality with a defect concentration of $10^{17}\,cm^{-3}$ and a high optical sub-band gap absorption, planar polycrystalline Si layers perforated with periodic arrays of tapered microholes are composed of a compact crystalline structure and a defect concentration in the low $10^{16}\,cm^{-3}$ regime. The low defect concentration is equivalent to the one in planar state-of-the-art solid phase crystallized Si films and correlates with a low optical sub-band gap absorption. By complementing the experimental characterization with 3-dimensional finite element simulations, we provide the basis for a computer-aided approach for the low-cost fabrication of novel high-quality structures on large areas featuring tailored opto-electronic properties. © *2013 AIP Publishing LLC*. [http://dx.doi.org/10.1063/1.4829008]

## I. INTRODUCTION

The design of highly efficient Si-based photonic and photovoltaic devices necessitates the development of advanced light management strategies. Periodically structured systems have recently emerged as concepts for nano-photonic light harvesting in amorphous and crystalline Si solar cells that, in contrast to random structures, provide tunable degrees of freedom for an electro-optical device optimization.[1–7] Lithographic patterning, anisotropic etching procedures and vapor–liquid–solid processes have already been used for a successful implementation of periodic Si structures into photovoltaic devices.[1,2,6–8] However, these existing methods either rely on high-quality substrates or do not comply with the standards of a low-cost production process on large areas. This calls for the development of cost-effective methods to manufacture periodic Si architectures. By combining the high-rate deposition technique electron-beam evaporation with nanoimprint lithography, we have already developed a low-cost and easily scalable fabrication process in a self-organized crystallization process for periodic arrays of crystalline Si for light harvesting and photonic crystals operating in the visible and near-infrared wavelength region.[9,10] Nanoimprint lithography is a viable option for structuring large-area substrates with manifold design possibilities for photovoltaic and photonic applications, while the solid phase crystallization (SPC) of deposited amorphous silicon enables the fabrication of crystalline thin film Si solar cells on glass with record module efficiencies of up to 10.5%.[3,11–15] However, in order to realize cost-effective, scalable and yet high-quality structures by employing this inexpensive fabrication technique, knowledge-based approaches are required that complement the predictive power of computer-aided design strategies with cutting-edge characterization tools.

In this contribution, we determine essential design parameters for large-area high-quality periodic Si microhole arrays on nanoimprinted sol-gel coated glass, by systematically correlating their structural and optical properties to their deep-level defect characteristics, which are a direct measure for the electronic quality. By complementing the experimental optical characterization with 3-dimensional finite element (FEM) simulations, we provide the basis for a computer-aided approach for the design of novel structures featuring tailored opto-electronic properties.

## II. PREPARATION OF PERIODICALLY STRUCTURED SI FILMS

Figure 1(a) illustrates a schematic of the preparation process of periodic Si architectures on glass. Various master

[a)]Author to whom correspondence should be addressed. Electronic mail: tobias.sontheimer@helmholtz-berlin.de

 

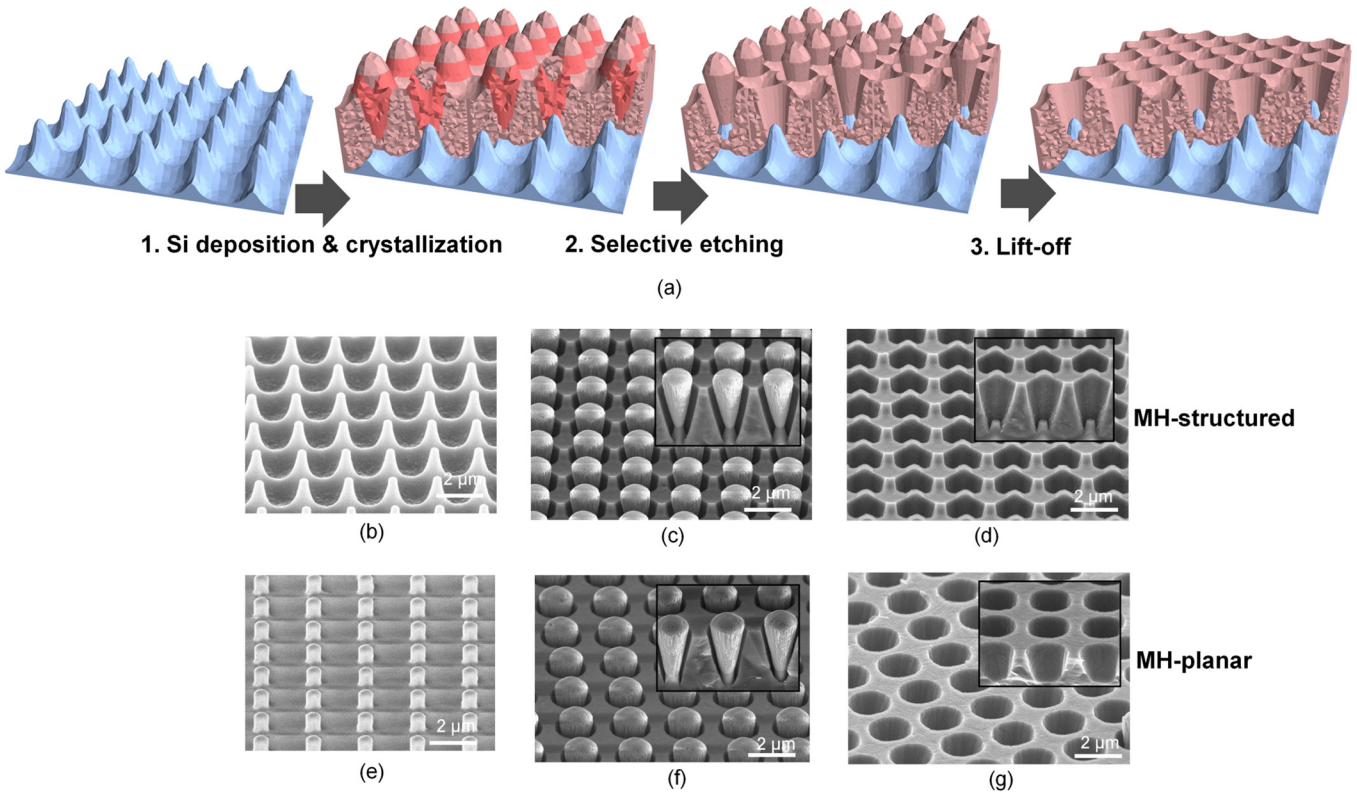


FIG. 1. (a) Fabrication process for Si structures and microhole arrays. The sol-gel is illustrated in blue, while Si is red. Porous amorphous regions are highlighted in bright red. (b) and (e) display SEM images of sol-gel templates with slanted flanks und u-shaped valleys and sol-gel cylinders protruding from a planar layer, respectively. (c) and (d) show the Si structure and tapered microhole arrays embedded in a structured base layer (MH-structured) based on a u-shaped sol-gel layer, respectively. (f) and (g) display the Si structure and the final microhole arrays perforating a planar Si base layer based on a sol-gel template with well defined cylindrical features (MH-planar).

stamps with a 2-dimensional periodic structure provide the desired pattern for the nanoimprint process and define the structure geometry. After a $(5 \times 10)$ cm$^2$ reusable polysiloxan replica stamp had been fabricated from the master structure, the replica stamp was pressed into a wet sol-gel film on glass. The sol-gel solution consists of nanoparticles synthesized with functionalized hybrid polymers and was applied to the glass by dip-coating. A short UV curing step of a few seconds prior to the stamp removal ensured that the imprint of the replicated structure was preserved. An additional thermal treatment enhanced the temperature stability of the imprinted structure and enabled its compatibility with the high temperatures involved in the poly-Si fabrication process.[16] Intrinsic amorphous Si layers with a thickness of 2.6 $\mu$m were deposited on the structured substrates by electron-beam evaporation at a deposition temperature of 300 °C and deposition rate of 300 nm/min, leading to periodic arrays of Si domes. Due to atomic shadowing effects during the deposition process, silicon grows in a void rich columnar morphology on steep edges and flanks of the imprinted pattern, allowing oxygen incorporation into the Si after the vacuum break.[17] Si deposited on flat areas of the substrate, however, exhibits a compact structure. This difference in the material structure enables a self-organized solid phase crystallization process at 600 °C in $N_2$ ambient, in which the compact material crystallizes, while the void and oxygen rich areas remain amorphous.[18] Afterwards, an etch solution was dropped onto the samples to remove porous amorphous material.[9] The resulting polycrystalline Si architecture on the structured sol-gel layer features arrays of truncated Si cones on the tips of the two-dimensional pattern and a polycrystalline base layer. The Si cones consist of a crystalline core, which is enclosed by a porous funnel with nanocrystalline rods. Finally, these Si cones are mechanically removed from the base layer in a simple lift-off process. The final structures consist of tapered microholes in a polycrystalline Si layer. The shape of the imprint stamp defines the structure of the Si architectures: A sol-gel texture consisting of tips with slanted flanks that are separated by u-shaped valleys (Fig. 1(b)) leads to the formation of a tapered microholes (MH) in a heavily structured layer (MH-structured). In contrast, a sol-gel pattern, which contains arrays of equidistant sol-gel cylinders emerging from a planar layer (Fig. 1(e)) gives rise to the formation of a planar Si base layer perforated with tapered holes (MH-planar). Figures 1(c), 1(d) and 1(f), 1(g) illustrate the fabricated structure before and after the lift-off process for both substrate types. To improve the structural quality of the material and saturate remaining defects, we applied state-of-the-art rapid thermal annealing at 950 °C for 1 min and a hydrogen passivation process in a parallel plate radio-frequency plasma setup at 600 °C for 15 min.[19,20] A conformal hydrogenated intrinsic amorphous Si layer was applied in a conventional parallel plate 13.56 MHz plasma enhanced chemical vapor deposition system at 130 °C for the passivation of interface-related defects.[21]

## III. ANALYTICAL TECHNIQUES

To elucidate the growth process of Si on the structured substrates, we performed cross-sectional transmission electron microscopy (TEM), employing a CM12 Philips TEM with supertwin lens modification, a $LaB_6$ cathode, and an acceleration voltage of 120 kV. We prepared 20–50 nm thick TEM specimens by manually cutting, polishing, and ionmilling. Recently conducted electron paramagnetic resonance (EPR) studies on planar poly-Si solar cells and numerical device simulations revealed that deep level paramagnetic intra-grain and grain boundary defects are major recombination centers in solid phase crystallized Si and hence the most important limitation of the electronic quality of poly-Si.[22] To evaluate the electronic quality of the manufactured structures, we conducted continuous wave EPR experiments at a microwave frequency of 9.8 GHz on a commercial Bruker ESP 300 spectrometer equipped with a $TE_{011}$ super high Q microwave resonator. The defect density was calculated based on a calibrated spin-counting procedure.[22] The effective material volume of the prepared structures was calculated, by constructing a 3-dimensional geometrical model from the cross-sectional TEM and SEM data.[23] The optical characteristics of the prepared microhole arrays were analyzed by performing absorption measurements on a Perkin Elmer Lambda1050 UV-VIS spectrometer with an integrating sphere, with the sample being mounted inside the sphere inclined at an angle of 10° to the incoming light beam.

## IV. CORRELATION BETWEEN STRUCTURAL, ELECTRONIC AND OPTICAL PROPERTIES

Figure 2 shows cross-sectional TEM images of a Si cone grown on a sol-gel template with tips with slanted flanks (Fig. 1(b)), and a tapered microhole structure (MH-planar) based on a sol-gel template with exclusively cylindrical features with normal angles (Fig. 1(e)), respectively. While the Si in cones is comprised of nanocrystalline rods in proximity to the interface (Fig. 2(a)), the tapered microhole arrays perforating a planar Si layer (MH-planar) exclusively consists of compact Si with a well-defined Si/air interface (Fig. 2(b)). The structural features of the Si architectures are in conformity with the growth characteristics of the physical vapor deposition of Si at inclined incidence.[17,18] While Si deposited at normal incidence has a compact structure, the density of the Si progressively decreases, as the angle of incidence increases, leading to porous structure consisting of individual columns.

Figure 3 depicts the total spin concentration $N_s$ as a function of the period of the prepared arrays. The gray bar highlights the reference value $N_s = (1.2 \pm 1.0) \times 10^{16}$ cm$^{-3}$ for simultaneously processed planar polycrystalline Si layers on glass, which is in accordance with the defect concentration in state-of-the-art solid phase crystallized Si material. Structures featuring defect-rich porous Si cones exhibit a defect concentration above $(9 \pm 2) \times 10^{16}$ cm$^{-3}$, exceeding the defect level of a planar reference by one order of magnitude. Tapered microhole arrays in a structured base layer (MH-structured) were found to have a defect concentration in the $10^{17}$ cm$^{-3}$ regime, as well. However, periodically arranged tapered

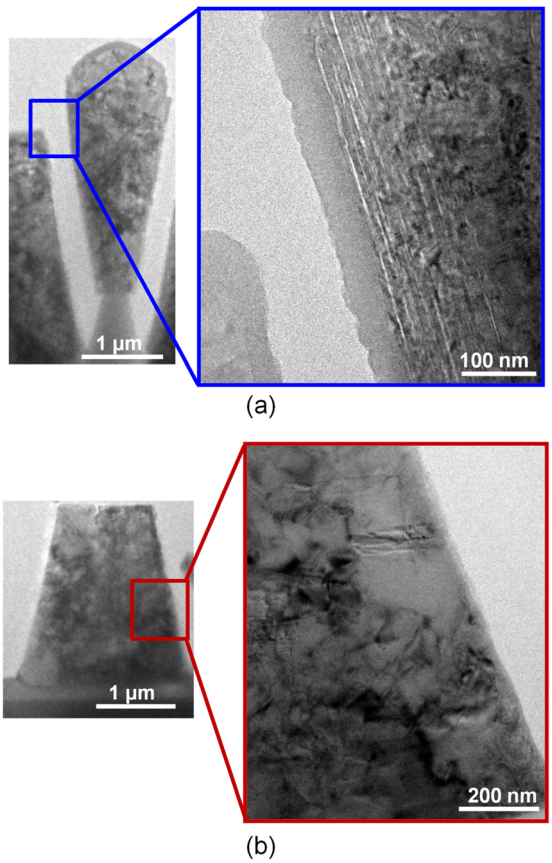


FIG. 2. (a) Cross-sectional TEM micrograph of a cone grown on a sol-gel template with tips with slanted flanks (Fig. 1(b)). (b) TEM micrograph of a tapered microhole structure (MH-planar) based a sol-gel template with exclusively cylindrical features with normal angles (Fig. 1(e)). The cone in part (a) is additionally covered with a 40 nm thick intrinsic amorphous hydrogenated Si layer.

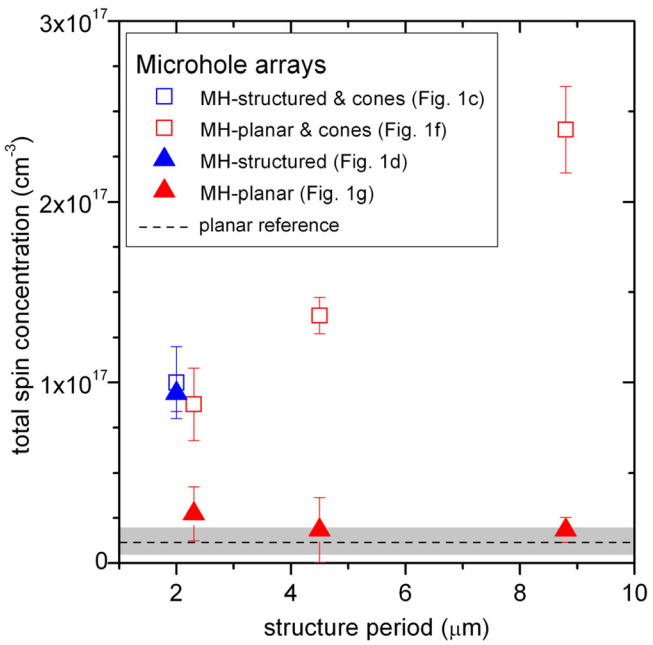


FIG. 3. Total spin concentration $N_s$ as a function of the Si structure period in comparison to a planar reference. The gray bar indicates the benchmark of a planar poly-Si thin film with $N_s = 1 \times 10^{16}$ cm$^{-3}$.

microholes in a planar base (MH-planar) with a period of 2.3 $\mu$m, 4.5 $\mu$m, and 8.8 $\mu$m yield a defect concentration of $(2.7 \pm 1.5) \times 10^{16}$ cm$^{-3}$, $(1.9 \pm 1.8) \times 10^{16}$ cm$^{-3}$, and $(1.8 \pm 0.7) \times 10^{16}$ cm$^{-3}$, respectively. These values resemble defect concentrations of planar Si layers on glass. Consequently, on the basis of an imprint structure with cylindrical tips on a planar sol-gel layer, we can design periodically structured Si with high electronic quality. The fact that the measured defect concentration is independent of the period of the structure, i.e., of the respective surface-to-volume ratio, confirms that interface-related defects have a negligible contribution to the total defect concentration. The high defect concentration of the microhole arrays in structured Si (MH-structured) and architectures with cones is ascribed to the growth characteristics of physical vapor deposition of silicon at intermediate angles of incidence, at which Si crystallizes but still retains the porous structure (Fig. 2(a)).

Figure 4 shows absorption spectra in the long wavelength and sub-band gap region of microhole arrays in structured Si (MH-structured) with a 2 $\mu$m period with $N_s = (9 \pm 1) \times 10^{16}$ cm$^{-3}$, microhole arrays (MH-planar) with high electronic quality with $N_s = (2.7 \pm 1.5) \times 10^{16}$ cm$^{-3}$ with 2.3 $\mu$m-periodic pattern and a planar reference ($N_s = (1.2 \pm 1.0) \times 10^{16}$ cm$^{-3}$) with an equivalent effective Si volume. The experimentally observed absorption beyond 1130 nm is caused by defect absorption, which is additionally amplified by the light path enhancement (LPE) provided by the structures. This detected optical sub-band gap absorption is in agreement with the trend of the defect concentration measured by EPR. Whereas a high $N_s = (9 \pm 1) \times 10^{16}$ cm$^{-3}$ corresponds to a high absorption at 1150 nm of 5%, the low $N_s = (2.7 \pm 1.5) \times 10^{16}$ cm$^{-3}$ of the MH-planar structure corresponds to a sub-band gap absorption which is similar to the absorption of the planar reference. The low sub-band gap absorption of the microhole arrays in a planar Si film is correlated with low dielectric losses in the near infrared region. Such low absorption properties are not only a crucial prerequisite for high-quality photovoltaic devices, but are also required for application in silicon based photonic crystal and photonic circuit fabrication, as high quality factor modes can only be achieved using low-loss materials.[10,24]

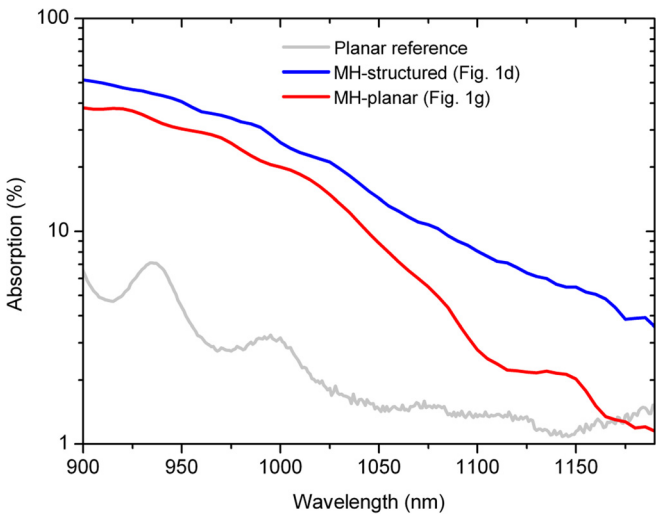


FIG. 4. Optical absorption spectra of defect-rich Si microhole arrays in a structured base layer with a 2 $\mu$m period (blue) and high-quality tapered microhole arrays in a planar base layer as a function of the wavelength of the incident light in comparison to a planar reference (gray).

## V. 3-DIMENSIONAL FEM SIMULATIONS

To establish a bottom-up approach for an electro-optical design optimization, we complemented the experimental analysis of the tapered microhole arrays in a planar base layer (MH-planar) with 3-dimensional FEM simulations based on optical parameters of crystalline Si and a 3-dimensional geometrical model, which was constructed from cross-sectional SEM and TEM images.[23] As in our previous publications,[23,25] we employ the finite element software JCMsuite[26] for solving the time-harmonic Maxwell's equations on space discretized geometrical models, with the adaptation that we incoherently couple a glass layer to the finite element model of the silicon structures. This coupling allows us to estimate light trapping effects within the substrate layer and has proven beneficial for the prediction of experimental results. For the illumination conditions and the scatterer studied here, this modification was not very important for obtaining a satisfying comparability to the experimentally measured absorptance. A maximum absorption of only 7% at 900 nm wavelength stems from multiple passes inside the finite substrate layer. Figure 5 illustrates the experimental and simulated optical absorption spectra of microhole arrays. The simulated results obtained for a plane wave light source at normal incidence from the coated side of the substrate are in perfect accordance with the experimental absorption up to 1050 nm. The less pronounced interference patterns in the measured absorption spectrum in comparison to the simulated spectrum might be ascribed to slight irregularities of the structure and to averaging effects due to the band width of the monochromator used in the experimental setup. On the basis of the experimentally derived design parameters for high-quality microhole arrays, 3-dimensional FEM simulations allow us to predict a structure with optimized optical properties. The simulated optical design can

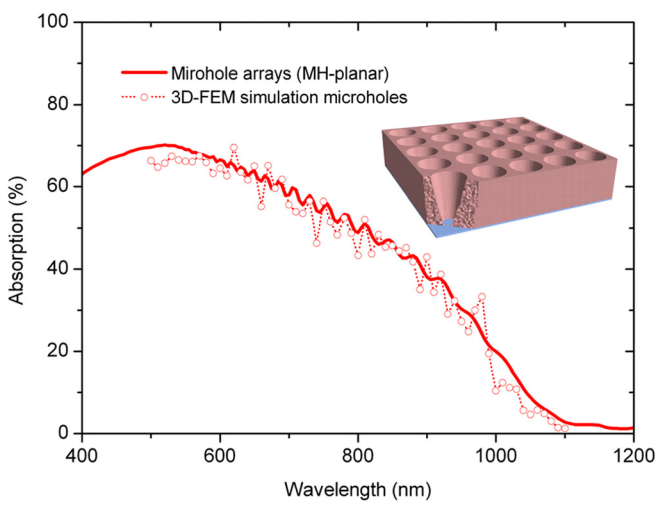


FIG. 5. Measured and simulated optical absorption of high-quality tapered microhole arrays with a 2.3 $\mu$m period.

finally be used to manufacture tapered microhole arrays with optimal opto-electronic properties.

## VI. CONCLUSION

We correlated the structural and optical properties with the deep-level defect characteristics of tailored Si microhole arrays on nanoimprinted glass. On the basis of this experimental analysis complemented with FEM simulations, we were able to reveal the structure opto-electronic function relationship in novel scalable Si microhole arrays. Tailored polycrystalline Si layers perforated with periodic arrays of tapered microholes (MH-planar) consist of exclusively compact crystalline Si and exhibit a defect concentration which is equivalent to a state-of-the-art planar reference sample in the low $10^{16}\,cm^{-3}$ regime. These electronic parameters are in accordance with the optical sub-band gap absorption. The optical absorption of the microhole arrays with a 2.3 $\mu$m pitch at wavelengths from the visible range up to 1000 nm shows an excellent agreement with 3-dimensional Finite Element Method simulations. However, the impact of our study goes even beyond this important result. The presented analyses and implemented simulation tools provide the basis for a predictive computer-aided approach for the design of novel structures featuring tunable opto-electronic properties. The presented approach is not limited to the design of light harvesting structures in next-generation solar cells, but may be used to tailor large-area 2D photonic crystal waveguides with low-loss propagation in the telecommunication wavelength regime.

## ACKNOWLEDGMENTS

We are indebted to Stefan Common and Erhard Conrad for their assistance with sample preparation. We are grateful to C. Klimm and U. Bloeck for SEM and TEM analyses, and thank L. Korte for discussions. V. Preidel acknowledges SCHOTT AG for financial support. The German Federal Ministry of Education and Research (BMBF) is acknowledged for funding the research activities of C. Becker in the Program NanoMatFutur (No. 03X5520).

[1]Z. Yu, A. Raman, and S. Fan, Opt. Express **18**, A366–A380 (2010).
[2]J. Zhu, C. Hsu, Z. Yu, S. Fan, and Y. Cui, Nano Lett. **10**, 1979–1984 (2009).
[3]C. Battaglia, C.-M. Hsu, K. Söderström, J. Escarré, F.-J. Haug, M. Charrière, M. Boccard, M. Despeisse, D. T. L. Alexander, M. Cantoni, Y. Cui, and C. Ballif, ACS Nano **6**(3), 2790–2797 (2012).
[4]S. Mokkapati and K. R. Catchpole, J. Appl. Phys. **112**, 101101 (2012).
[5]O. Isabella, S. Solntsev, D. Caratelli, and M. Zeman, Prog. Photovoltaics **21**, 94 (2013).
[6]S. W. Schmitt, F. Schechtel, D. Amkreutz, M. Bashouti, S. K. Srivastava, B. Hoffmann, C. Dieker, E. Spiecker, B. Rech, and S. H. Christiansen, Nano Lett. **12**, 4050 (2012).
[7]H. Sai, K. Saito, N. Hozuki, and M. Kondo, Appl. Phys. Lett. **102**, 053509 (2013).
[8]M. D. Kelzenberg, S. W. Boettcher, J. A. Petykiewicz, D. B. Turner-Evans, M. C. Putman, E. L. Warren, J. M. Spurgeon, R. M. Briggs, N. S. Lewis, and H. A. Atwater, Nature Mater. **9**, 239 (2010).
[9]T. Sontheimer, E. Rudigier-Voigt, M. Bockmeyer, C. Klimm, P. Schubert-Bischoff, C. Becker, and B. Rech, Phys. Status Solidi (RRL) **5**, 376 (2011).
[10]C. Becker, D. Lockau, T. Sontheimer, P. Schubert-Bischoff, E. Rudigier-Voigt, M. Bockmeyer, F. Schmidt, and B. Rech, Nanotechnology **23**, 135302 (2012).
[11]L. J. Guo, Adv. Mater. **19**(4), 495–513 (2007).
[12]V. E. Ferry, M. A. Verschuuren, H. B. T. Li, R. E. I. Schropp, H. A. Atwater, and A. Polman, Appl. Phys. Lett. **95**, 183503 (2009).
[13]C. Battaglia, J. Escarré, K. Söderström, M. Charrière, M. Despeisse, F.-J. Haug, and C. Ballif, Nature Photon. **5**, 535 (2011).
[14]T. Sontheimer, C. Becker, F. Ruske, C. Klimm, U. Bloeck, S. Gall, O. Kunz, T. Young, R. Egan, J. Hupkes, and B. Rech, in *Proceedings of the 35th IEEE Photovoltaic Specialists Conference* (IEEE, 2010), p. 614.
[15]M. A. Green, K. Emery, Y. Hishikawa, W. Warta, and E. D. Dunlop, Prog. Photovoltaics **21**, 1–11 (2013).
[16]E. Rudigier-Voigt, M. Bockmeyer, V. Hagemann, and S. Bauer, in *Proceedings of the 24th European Photovoltaics Solar Energy Conference, Hamburg, Germany* (EU-PVSEC Proceedings, 2009), p. 2884.
[17]A. G. Dirks and H. J. Leamy, Thin Solid Films **47**, 219 (1977).
[18]J. J. Merkel, T. Sontheimer, B. Rech, and C. Becker, J. Cryst. Growth **367**, 126 (2013).
[19]B. Rau, T. Weber, B. Gorka, P. Dogan, F. Fenske, K. Y. Lee, S. Gall, and B. Rech, Mater. Sci. Eng., B **159–160**, 329 (2009).
[20]B. Gorka, B. Rau, P. Dogan, C. Becker, F. Ruske, S. Gall, and B. Rech, Plasma Processes Polym. **6**, S36 (2009).
[21]T. F. Schulze, H. N. Beushausen, C. Leendertz, A. Dobrich, B. Rech, and L. Korte, Appl. Phys. Lett. **96**, 252102 (2010).
[22]M. Fehr, P. Simon, T. Sontheimer, C. Leendertz, B. Gorka, A. Schnegg, B. Rech, and K. Lips, Appl. Phys. Lett. **101**, 123904 (2012).
[23]D. Lockau, T. Sontheimer, C. Becker, E. Rudigier-Voigt, F. Schmidt, and B. Rech, Opt. Express **21**, A42–A52 (2013).
[24]M. M. Sigalas, K. M. Ho, R. Biswas, and C. M. Soukoulis, Phys. Rev. B **57**, 3815 (1998).
[25]D. Lockau, T. Sontheimer, V. Preidel, C. Becker, F. Ruske, F. Schmidt, and B. Rech, in *Optical Properties and Limits of a Large-Area Periodic Nanophotonic Light Trapping Design for Polycrystalline Silicon Thin Film Solar Cells* (Mater. Res. Soc. Symp. Proc., 2013), Vol. 1493.
[26]S. Burger, L. Zschiedrich, J. Pomplun, and F. Schmidt, in *Integrated Photonics and Nanophotonics Research and Applications* (Optical Society of America, 2008), paper no. ITuE4.